water

MDPI

Article

Induced Circulation by Plunging and Submerged Jets in Circular Water Storage Tanks Using CFD

Nuno M. C. Martins *,† **and Dídia I. C. Covas** †

CERIS, Instituto Superior Técnico, Universidade de Lisboa, Av. Rovisco Pais 1, 1049-001 Lisboa, Portugal; didia.covas@tecnico.ulisboa.pt

* Correspondence: nunomiguelmartins@tecnico.ulisboa.pt

† These authors contributed equally to this work.

Abstract: Water circulation in storage tanks significantly impacts water quality in distribution networks since old water tends to have low residual chlorine concentrations that are insufficient to neutralize microbial regeneration. Their large capacity and long residence times result in uneven mixing, which can accelerate the disinfectant decay and the formation of potentially carcinogenic disinfection by-products. The phenomenon is strongly related to the tank inflow conditions, since there are no active mixing devices. This paper presents a comprehensive analysis of the flow dynamics in circular storage tanks using a three-dimensional computational fluid dynamics model. The main motivation is that the inflow—which mixing processes rely on—strongly influences the circulations. The numerical analysis provided includes a thorough investigation of interest in understanding flow dynamics for two inflow configurations: (i) the plunging jet modelling and comparison with published experimental data and (ii) the submerged jet as an improvement measurement for these storage tanks.

Keywords: computational fluid dynamics; water storage tank; plunging jet; submerged jet; mixing conditions

Citation: Martins, N.M.C.; Covas, D.I.C. Induced Circulation by Plunging and Submerged Jets in Circular Water Storage Tanks Using CFD. *Water* **2022**, *14*, 1277. https://doi.org/10.3390/w14081277

Academic Editor: Stefano Alvisi

Received: 7 March 2022
Accepted: 12 April 2022
Published: 14 April 2022

1. Introduction

Water distribution networks are composed of assets that allow the water intake, treatment, transport, storage and delivery to consumers in quantity and with adequate pressure to satisfy demand. However, once the water leaves the treatment plant and enters the supply infrastructure, maintaining its quality is challenging for utility managers [1]. While the disinfectant decay in the water transport and distribution network is reasonably well known [2,3], the effect of storage on treated water quality is not fully understood [4,5]. It is believed that better water mixing in storage tanks guarantees better water quality and safer drinking water [6], although little is known about mixing regimes in general [7,8]. Water storage tanks aim to supply consumers in normal operating conditions regulating flow rate differences in transmission pipes and distribution networks, levelling off pressures to meet daily consumer demands, and providing emergency storage for firefighting and pumping disruptions [9]. These storage facilities are operated by controlling the water level [10]; however, their large capacities and long residence times, usually associated with uneven mixing, can significantly deteriorate the water quality supplied to the downstream network [11]. One of the most negative impacts is the loss of residual disinfectant (disinfectant decay), promoting microorganisms regrowth and increasing human pathogens' survival [9]. These circumstances result in the need for re-chlorination [12], resulting in the subsequent formation of potentially carcinogenic toxic by-products [13,14]. Improving mixing processes in existing storage tanks may be attained by installing an active mixing device such as an impeller or a turbine [15]. However, when these devices do not exist,

the mixing process in the storage tank strongly relies on jet mixers [16]. The jet momentum, M, is given by:

$$M = \frac{V_N^2 \pi D_N^2}{4} \quad (1)$$

where V_N = mean velocity in the nozzle and D_N = inlet nozzle diameter. Whenever a water flow through a nozzle (jet) encounters a large mass of undisturbed liquid, the jet forces the stored water into the storage tank, leaving a track of moving particles called the 'entrainment path'. The jet direction should ensure a long and unobstructed 'entrainment path' to improve the mixture [15]. However, the 'entrainment path' in a given storage tank geometry gives rise to a complex three-dimensional (3D) flow pattern, which is often difficult to characterise. This subject presents a significant concern to utilities as storage tanks have different sizes, geometries (circular, rectangular), installed features (with or without baffles; inlet–outlet configurations and sizes) and several size-to-ratio dimensions (water level/length $\lambda = H/D_T$. Each combination results in a different flow pattern, which is a decisive factor in the water mixing in tanks [17]. Even experimental and field studies cannot fully describe and characterise the flow pattern since sampling techniques can only assess the water at specific locations and not in the entire tank volume since tracer tests are carried out at these points, which are insufficient to interpret the 3D flow pattern. Several authors have captured the complex flow pattern using several measurement techniques in small-scale models using Acoustic Doppler Velocimetry for volume sampling [18] and the 3D laser-induced fluorescence for plane sampling [19,20].

For this reason, several researchers focused on assessing and analysing the mixture quality by means of numerical models, such as computational fluid dynamics (CFD), which is largely used to simulate fluid flows [21–24]. Okita and Oyama [25] tested an extensive range of orifices for two small-scale circular tanks. These researchers concluded that the ratio between the tank diameter, D_T, and the nozzle diameter, D_N, is related to the mixing time as a function of the inflow (nozzle) characterised by the Reynolds number, $Re = \rho V_N D_N/\mu < 4 \times 10^4$, in which μ = dynamic viscosity. Grayman et al. [15], using a small-scale model, proposed methods to support the design and operation of water storage tanks to reduce the risk of water quality degradation from poor mixing. Khan et al. [26] showed results of a 3D CFD model and concluded that the numerical model could accurately reproduce the flow patterns. Likewise, Marek et al. [27] compared the numerical concentration profiles with the experimental ones and concluded that 3D CFD model is able to simulate the complex effects of the flow. In addition, Zhang et al. [28] evaluated several locations of submerged nozzles with a numerical model to determine the ozone concentration and disinfectant contact time values, concluding that the modelling results agreed well with the full-scale experimental data.

In general, researchers observed that the flow pattern in storage tanks is highly dependent on the momentum of the inflow nozzle and the respective inflow orientation [29], the number of jets (single and multiple) [30] and the position of the jet with respect to the water level in the tank [31]. So far, a significant number of conditions have been studied for the nozzle positioned below the water level (submerged jet) in several directions and locations [9,20], while according to the authors' knowledge, no studies have been conducted in storage tanks with a plunging jet.

For these reasons, the current research aims to better understand the flow hydrodynamics (flow pattern) in circular storage tanks for two inflow configurations—above and below the water level—through a 3D CFD model. The nozzle above the water level is referred to as a plunging jet, while the nozzle below the water level is a submerged jet. The detailed information about flow patterns represents a valuable tool to establish the design and guidelines for operation and rehabilitation in order to improve the water mixture in storage tanks and, thus, assuring the safety of drinking water distribution networks.

The main innovative key features of this paper are: (i) the analysis of the flow pattern of a plugging jet in a circular storage tank validated by available laboratory data; (ii) the flow pattern analysis of a submerged jet for the same geometry as an improvement mea-

surement of water mixture; and (iii) velocity fields comparison of both inflows: plunging and submerged jet.

2. Background Jet Theory

2.1. Plunging Jet

A circular nozzle positioned above the water level generates an axisymmetric jet with a velocity, V_N^*, a diameter, D_N^*, and an angle with the horizontal plane, θ_N^* (Figure 1). As the stream leaves the nozzle, a smooth and cylindrical shape jet is established. The jet is immediately subjected to gravity forces and surface tension: gravity adds a vertical velocity component, which causes the water jet to fall, while the surface tension maintains the jet shape by the molecular attraction forces of the water (cohesion). While the jet falls, the gravity force increases its velocity, causing the jet diameter to decrease (maintaining the same flow rate). Due to the surface tension, the cylindrical jet shape surface behaves as an elastic membrane, stretching and subjecting the region with more curvature. These effects increase as the jet develops and become more prominent. Due to the turbulent velocity component, the well-defined jet may break into multiple droplets [32] until it reaches the water level, depending on the flow rate and the vertical distance between the nozzle and the water surface.

As the jet attains the water level, the phenomenon is mainly influenced by the gravity force, being characterised by the impact angle, θ_P, the diameter, D_P, and the mean velocity, V_P (Figure 1). The plunging jet momentum results in the penetration of the stream into the pool of water (Figure 1a) or droplets being formed (Figure 1b), creating a meniscus void, with a cylindrical shape, in the pool surface. The air entrainment results from the volatility of the air–water interfaces, which is also known as Helmholtz–Taylor hydrodynamics instability [33]. The air entrainment by a plunging jet is frequently encountered in practice, namely, in cases of fluid aeration [33–35].

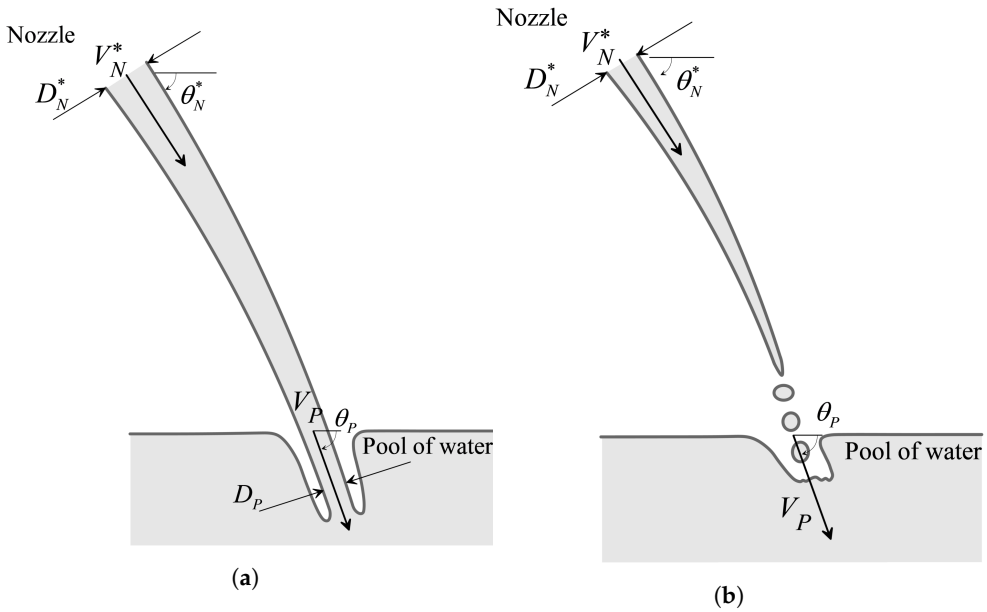

Figure 1. The plunging liquid jet when it: (**a**) maintains the cylindrical shape; (**b**) breaks into droplets.

In addition, the falling jet causes a deviation from the state of equilibrium in the tank (in the gravitational field), which generates an oscillatory motion due to the gravity and surface tension (capillary forces). This motion propagates along the water surface in waves known as gravity–capillary waves, which are common in nature and often referred to as ripples [36,37].

2.2. Submerged Jet

A submerged circular nozzle generates an axisimmetric jet with a mean velocity V_N and a diameter D_N which, independently of the initial flow regime, being laminar or turbulent, becomes turbulent at a certain distance from the nozzle [38]. The discontinuity between the jet mean velocity and the water in the tank at rest is highly unstable, and due to viscosity, the neighbouring fluid layers are increasingly drawn into the motion, embodying part of the fluid at rest and sweeping it along, giving rise to a mixing layer downstream of the nozzle (Figure 2). The thickness of the mixing layer, also called the shear layer, increases with the distance from the nozzle [39]. In the mixing layer, coherent structures (vortices) are formed, and their sizes are of the order of magnitude of the layer thickness—the fluid particles from the tank carried by the jet increase the mass flow. Consequently, the jet width spreads out, $D_S > D_N$, taking the shape of a bell, and the mean velocity of the flow, V_S, decreases with the increasing distance from the nozzle [25].

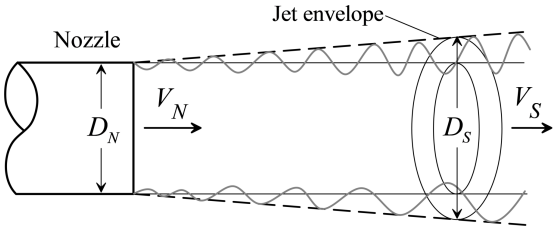

Figure 2. Jet surface roughness—schematics.

3. Models Description

Portugal's most common drinking water storage tanks are placed in-ground, have a circular cross-section without internal baffles, and a ratio between tank diameter and water height, $0.04 < H/D_T < 1.85$ [40]. The nozzle is typically located above the water level (as a plunging jet) to separate the storage tank from the upstream transmission pipeline, avoiding emptying the tank if a sudden accident occurs and is not timely detected.

To investigate the water mixing and renewal in storage tanks, an experimental facility designed for tracer tests in the small-scale storage tanks have been assembled in the Hydraulics Laboratory of Instituto Superior Técnico, Universidade de Lisboa, as part of the IMiST research project (FCT PTDC/ECI-EGC/32102/2017). Qualitative evaluation of preferred flow paths is presented in Figure 3a, where the inflow and outflow are located on opposite sides (configuration A in Pinheiro et al. [41]) is used to validate CFD results for the plunging jet configuration (Figure 3b). The inflow below the water level (Figure 3c) is numerically analysed and presented herein as an improvement measurement not tested in the experimental facility, although CFD model configurations, qualitatively evaluated with laboratory data, are used in both inflow positions: above the water level (plunging jet, the one tested in the experimental facility) and below the water level (submerged jet).

This numerical study aims at assessing the main effects of the inflow position in the flow pattern and the water mixing and renewal. Analyses are carried out for a constant water level, for which the inlet flow rate equals the outlet flow rate.

The tank diameter $D_T = 392$ mm and the water level $H = 60$ mm. The inlet nozzle has a diameter $D_N = 4$ mm and a pipe wall thickness $e = 1$ mm; the shape of the jet is defined by the circular cross-section (pipe). The jet is horizontally oriented, protrudes 4 mm from the tank wall, and the respective axis is positioned 17 mm above the water level-plunging jet (P), $z_P = 77$ mm. The submerged jet (S) is positioned 30 mm below the water level, $z_S = 30$ mm. The inlet flow rate equals the outlet flow rate, which corresponds to 9.4 l/h, with a $V_N = 0.208$ m/s, $Re = 827$ (<2000, laminar flow in the nozzle). The tank dimensions were determined by downscaling sizes and shapes of drinking water storage tanks most common in Portugal, based on Froude's law for 1:100 geometric scale [41].

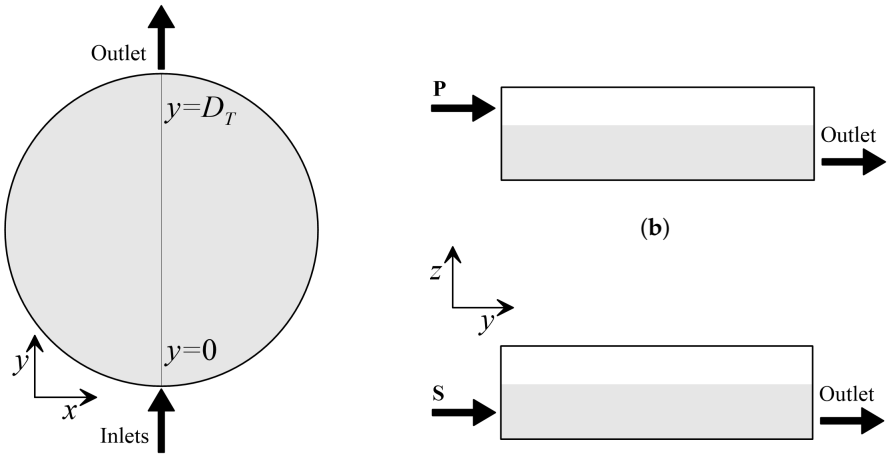

Figure 3. Inlet–outlet configuration–schematics: (**a**) top view; (**b**) plunging jet (P); and (**c**) submerged jet (S).

4. Computational Fluid Dynamics Model

4.1. Introduction

The OpenFOAM is a free, high-level language CFD library. The applications created by libraries are divided into solvers and utilities. The former performs the actual calculations that closely parallel the description of continuum mechanical problems, and the latter provides a range of functionalities for pre- and post-processing utilities [42].

4.2. Mesh

The snappyHexMesh is a pre-processing tool that considers a background mesh (pure hex mesh), generated by the blockMesh utility, and it chisels and refines it into the fluid domain defined by computer-aided software. It follows three meshing steps: (i) the cells of the background mesh are deleted beyond the fluid domain boundaries (castellation); (ii) the cells are reconstructed to approximate edges to the fluid domain boundaries (snapping); and (iii) the additional layers are generated in the boundary region (layering).

The final mesh is hex-dominant, refined in the tank's walls, inlet and outlet regions, in the air–water interface and where high-velocity gradients are expected (Figure 4)—resulting in a mesh that is characterised by 1.4 million mainly hexahedral cells with 1.5 million points of calculus, and by the minimum and maximum volumes of cells of 9.4×10^{-13} and 2.3×10^{-7}, respectively.

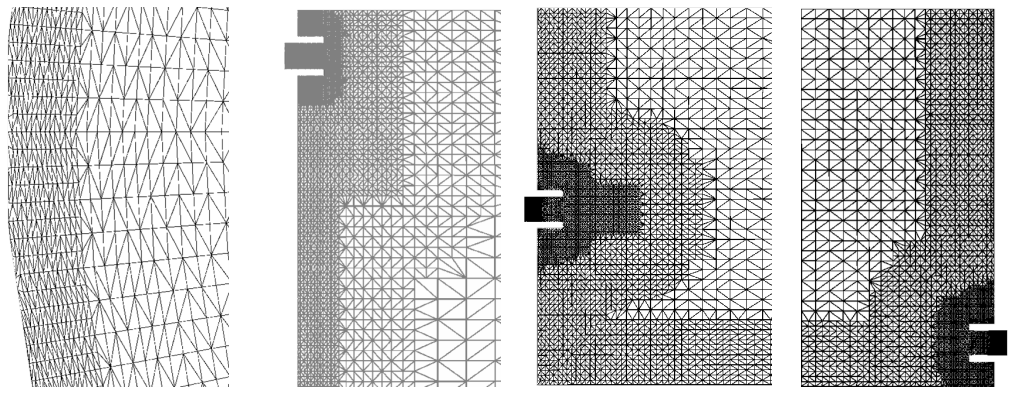

Figure 4. Mesh refinements: (**a**) top view; (**b**) nozzle above the water level; (**c**) nozzle below the water level; and (**d**) outlet region.

Even if the inflow is laminar, the behaviour of particles is complex, with jets (plunging and submerged) leading the flow. However, the circulating flow, mainly near the walls, is predominant and defines the flow pattern.

Less refined meshes settings were analysed and tested (higher minimum and maximum volume of cells); however, the flow pattern obtained by the CFD data did not follow the observed by recorder images of the movement of the dye tracer solution in the laboratory [41]. For the sake of brevity, the analyses of less refined meshes are not presented herein.

4.3. Multiphase Flow

For the flow pattern analysis, a multiphase solver has been used. For each phase, the solver multiphase InterFoam captures the interfaces between two (water and air) and includes surface tension and contact angle effects. It uses the finite volume along with the volume of fluid method. The starting point is the equations of mass conservation (continuity),

$$\nabla \bullet \mathrm{V} = 0 \tag{2}$$

and momentum,

$$\frac{\partial \rho \mathrm{V}}{\partial t} + \nabla \bullet (\rho V \otimes V) = \nabla \bullet \tau - \nabla p + \rho \mathrm{f}_b \tag{3}$$

where V = velocity vector shared by the two phases throughout the flow domain, γ = phase fraction, τ = viscous stress tensor given by $2\mu\mathrm{S} - \frac{2}{3}\mu(\nabla \bullet V)I$, with the mean rate of the strain tensor $\mathrm{S} = 0.5\left[\nabla V + (\nabla V)^T\right]$, and $\mathrm{I} = \delta_{ij}$, p =pressure, f_b are body forces per unit mass, which includes gravity, g, and surface tension effects at the interface [43]. The volume fraction transport equation is given by:

$$\frac{\partial \gamma}{\partial t} + \nabla \bullet (\gamma V) + \nabla \bullet [\gamma(1-\gamma)V_r] = 0 \tag{4}$$

where phase γ can take values within the range $0 \leq \gamma \leq 1$ and V_r = relative velocity of the phases; the solution of γ is achieved through a multidimensional universal limiter for explicit solution, which is an explicit solver based on the Flux-Corrected Transport technique [44].

The physical properties are calculated as weighted averages based on the distribution of the water volume fraction, thus being equal to the properties of each fluid in their corresponding occupied regions and varying only across the interface:

$$\rho = \rho_w \gamma + \rho_a(1-\gamma) \tag{5}$$

$$\mu = \mu_w \gamma + \mu_a(1-\gamma) \tag{6}$$

where the subscripts w and a refers to water and air, respectively. To close the problem, it is necessary to specify the initial and boundary conditions in space in time [45].

For the simulation, an unsteady Reynolds-Averaged Navier–Stokes for turbulence is adopted. The gradient and divergence schemes used were the Gaussian integration with linear interpolation. The SST k-ω model is selected by its main feature: it is a two-equation eddy viscosity hybrid model that combines the use of Wilcox k-ω and the k-ε models. The SST k-ω model activates the k-ω model near the wall and the k-ε model away from it; this zonal formulation is based on blending functions [46]. The SST k-ω model is used when the flow is affected by a solid or a surface (e.g., aerodynamics applications and 'Coanda effect')—justifying the need for a refined mesh near the wall.

Convergence can be assessed by progressively tracking the imbalances (residuals) accentuated by each iteration. A convergence solution is achieved when the residuals fall below the convergence criterion of 10^{-9}.

5. Results and Discussion

5.1. Plunging Jet

In a plunging jet, the water enters the tank by the horizontally oriented nozzle. The flow inside the nozzle is laminar ($Re_N = 827$) and as the cylindrical jet exits the nozzle, it is immediately subjected to gravity and surface tension forces. The gravity is responsible for the fall of the jet (i.e., vertical velocity component), while the surface tension maintains the initial shape of the jet (Figure 5).

The jet is immediately pushed downwards and, due to the adhesion of the water molecules to other substances or materials, the jet attaches to the inferior wall of the nozzle tip (Figure 5), adding a horizontal velocity component in the wall direction. This phenomenon is known as the 'Coanda effect', which is the tendency of a stream to stay attached to a convex surface. This attachment pulls in the flow, adding a horizontal velocity component in the wall direction [47,48].

As the jet continues, the water molecules attracted to the nozzle tip are also attracted to each other, resulting in a distortion of the jet shape (Figure 5). The 'Coanda effect' can be noticed by the water molecules' attractiveness to the nozzle's tip, altering the cylindrical shape to a flattened and angled jet. This effect is responsible for an early break of the jet into droplets of smaller total area surface [49].

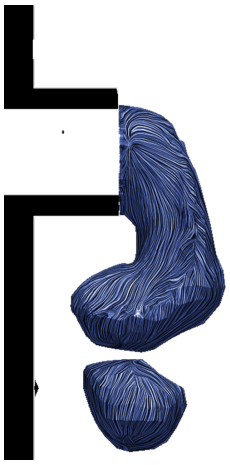

Figure 5. Plunging jet.

As a droplet penetrates the pool of water, it leaves a void on the surface of the pool (Figure 3b). The thin layer of air along the droplet surface is transported below the water level, forming small air bubbles [50]. These air bubbles are dragged downwards and are slowed down by buoyancy forces that push them upwards. This instability is responsible for most of the air entrainment. As a result, some air bubbles emerge at the water surface, where they rapidly coalesce, while some are dragged by the flow [51]. This agitation causes the jet to penetrate the surface of the pool of water and become more turbulent; however, it will not reach very deep and represents a considerable loss in the dynamic pressure [52].

The droplets' impact generates an oscillatory motion in the surface of the pool in the form of gravity–capillary waves (*ripples*) [53] that travel radially from the tank walls towards the centre of the circular storage tank (Figure 6).

The flow pattern starts to be established. Due to the 'Coanda effect' in the tank wall, the water from the jet progresses clung to the tank walls, symmetrically, in the left and right directions (Figure 6a–c). Pinheiro et al. [41], using a visual tracer (rhodamine solution), observed this flow pattern.

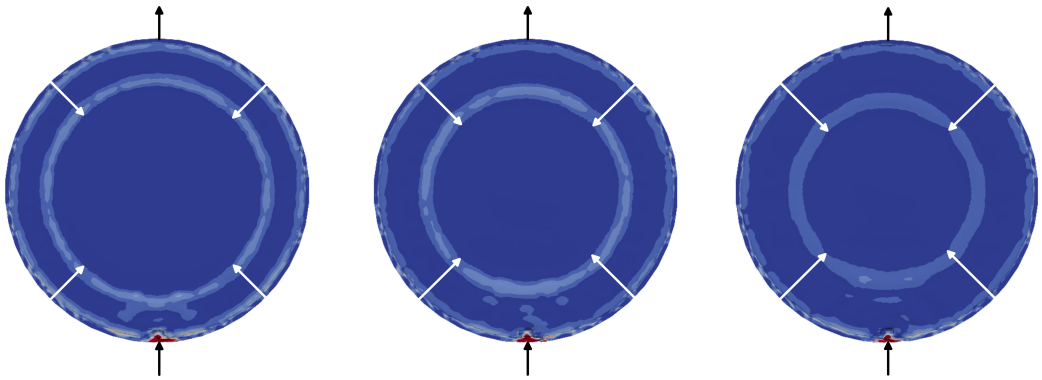

(**a**) (**b**) (**c**)

Figure 6. Wave propagation at different time steps from the beginning of the flow: (**a**) t_1 =0.50 s; (**b**) t_2 =0.60 s; and (**c**) t_3 =0.70 s.

The flow pattern results from a combination of the inlet and the outlet position and the tank configuration (circular cross-section and no baffle structures). The evolution in the initial time steps is always close to the wall due to the 'Coanda effect'. The 'Coanda effect' occurs when fluid is closely projected to a surface (wall, ceiling, pipe). When this happens, the fluid tends to cling to the surface as it moves due to the local pressure drop caused by the acceleration of the flow around a solid surface, allowing the fluid to remain clung. However, the flow gains a downward component, developing the flow pattern presented in Figure 6. Due to the inlet position above the water level, the jet falls near the wall and adheres while continuing to progress. After a short period, the flow starts to feel the reverse flow and the initial phase of the flow pattern; this effect can be observed in detail in Figure 7.

After 50 s of simulation, the flow pattern is beginning to be established. It is possible to observe that due to the dynamic pressure of the inflow, the undisturbed particles in the tank are pushed against the tank walls. This results in a reverse flow (from the outlet to the inlet), colliding with the inflow. As the reverse flow progresses, it pushes the inflow.

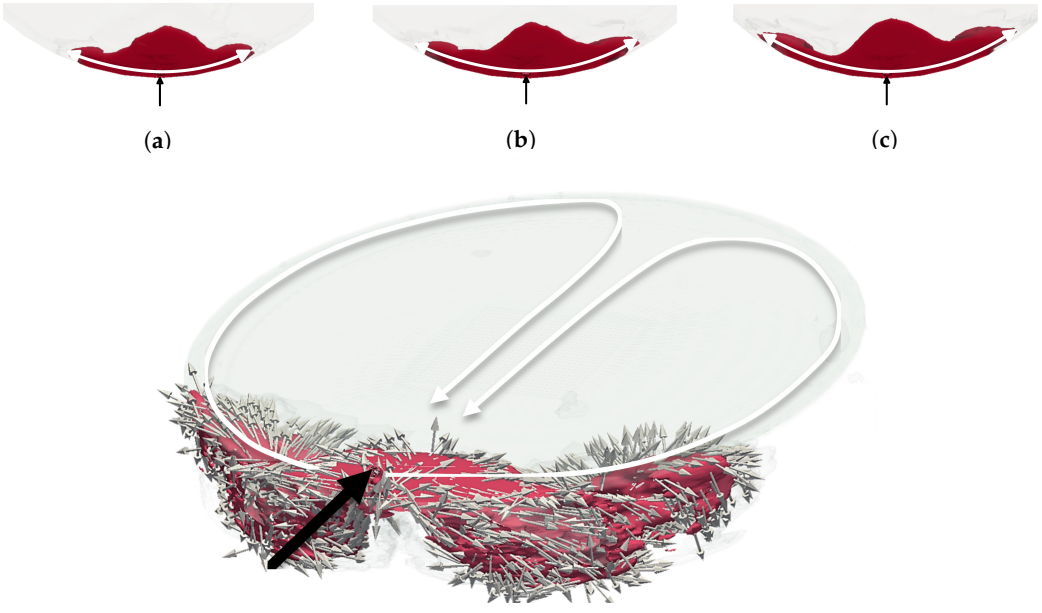

(**a**) (**b**) (**c**)

(**d**)

Figure 7. Water progression in the pool from the jet at (**a**) 9 s; (**b**) 12 s; (**c**) 15 s; (**d**) 50 s.

At 200 s, the 3D steady pattern is established in the tank, challenging to characterise; the inflow continues to cling to the wall, and it is disturbed and pushed down by the

reverse flow. Figure 8 presents velocity vectors at three tank heights, $z =$ ¼, ½ and ¾ H of the water level, corresponding to $z = 0.015$, 0.030 and 0.045 m, respectively (Figure 8a–c). The flow pattern near the bottom is different from the one near the surface (Figure 8d). After 200 s, the flow pattern shows slight changes due to flow turbulence.

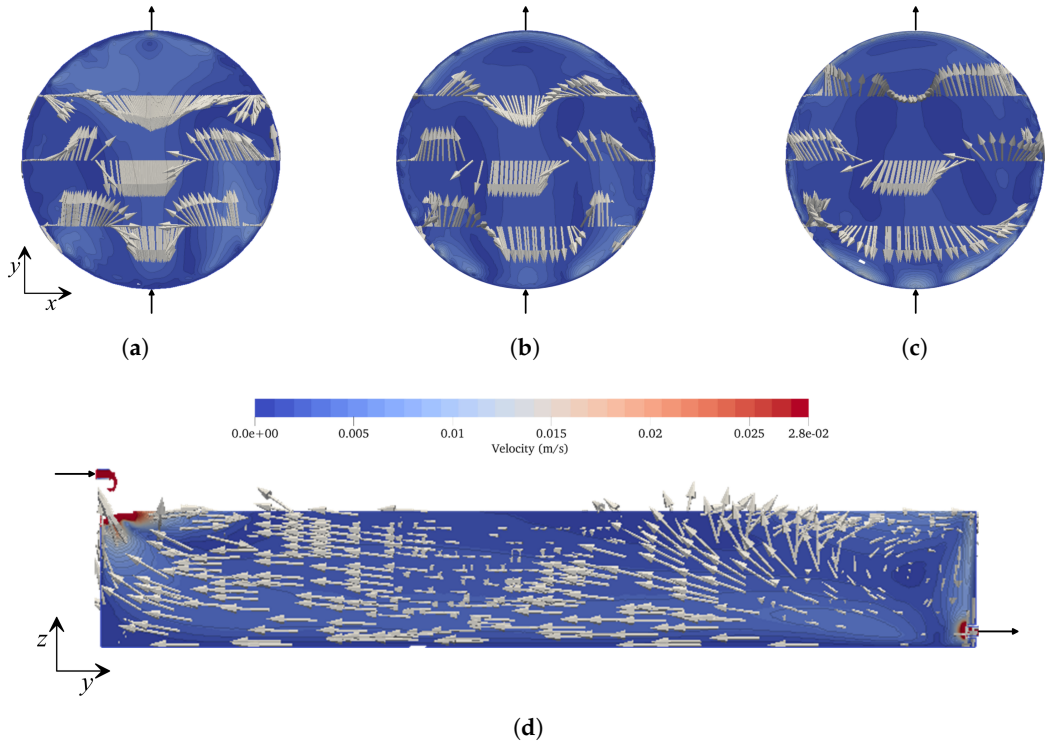

Figure 8. Plunging jet: velocity vectors and contours at 200 s in the horizontal plane at (**a**) $z = 0.25H$; (**b**) $z = 0.5H$; (**c**) $z = 0.75H$; and in the vertical plane at (**d**) $y = 0.5D_T$.

5.2. Submerged Jet

The nozzle is positioned below the water level, horizontally oriented at half of the total water height H, protruding 4 mm from the tank wall. In this configuration, the flow rate and the jet momentum are the same as in the plunging jet ($Re_N = 827$), which results in a cylindrical jet.

As the water jet leaves the nozzle (at time $t = 0$ s), the inflow has an immediate response by the surrounding particles. The entrainment path left by the jet is compensated by a reverse flow (Figure 9). In the surroundings of the entrainment path, fluid layers are continuously being added, reducing the jet mean velocity, which becomes more spread out. This is observed in Figure 9, as a 4 mm nozzle diameter results in a 20 times larger jet diameter at the centre of the tank (at $y =$ ½)

A 'zero velocity' region is observed between the 'entrainment path' and the reverse flow, and fluid layers are increasingly drawn into the motion, enlarging the entrainment path. When the inflow attains the tank wall ($y = D_T$), the flow pattern has been established. The high velocities are positioned in the centre (entrainment path) and are surrounded by a 'zero' velocity region, followed by a reverse flow. Note that there is no zero-velocities region, this region is concentrated between two streams with different directions that are highly unstable due to turbulence.

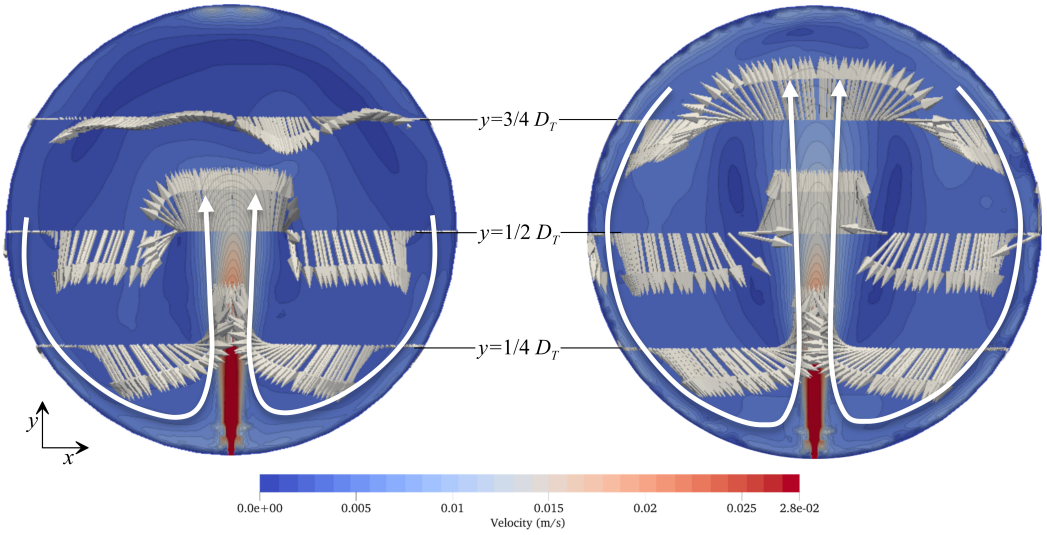

Figure 9. Plunging jet: velocity vectors and contours at $z = 0.5H$ at (**a**) 50 s; and (**b**) 150 s.

Two streams are observed (Figure 9): the one generated by the jet (entrainment path) and the other by the reverse flow that compensates. The flow pattern is established as the jet reaches the wall, which is symmetrical in the *y*-direction and divided into two parts. Due to the curved tank walls, the fluid clings to the surface as it moves ('Coanda effect'), generating a pressure drop at the surface, which allows the liquid to remain clung.

The main features of the flow pattern can be observed in Figure 10, in which velocities vectors are plotted at three heights, $z =$ ¼, ½ and ¾ H: for $z =$ ¼ H, the flow occurs clung to the wall, in the downward direction (Figure 10a); for $z =$ ½ H, the flow pattern seems to be more defined, with a lower downward flow rate than closer to the bottom (Figure 10b); finally, at $z =$ ¾ H, the flow pattern is mainly directed to the tank walls (Figure 10c).

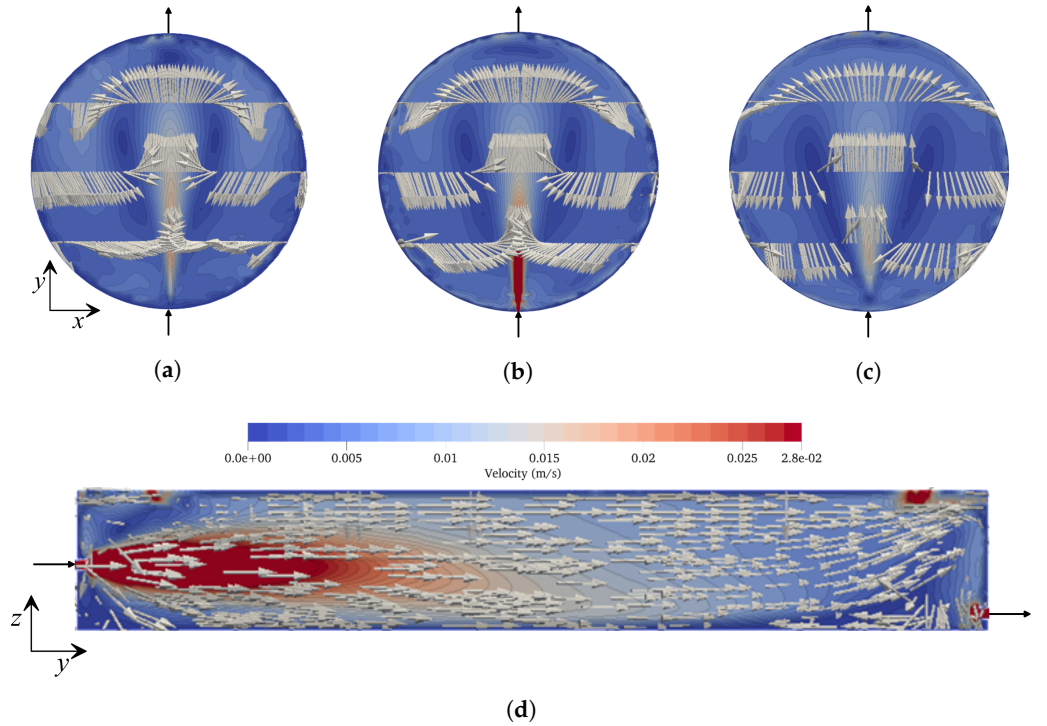

Figure 10. Plunging jet: velocity vectors and contours at 200 s in the horizontal plane at (**a**) $z = 0.25H$; (**b**) $z = 0.5H$; (**c**) $z = 0.75H$; and in the vertical plane at (**d**) $y = 0.5D_T$.

5.3. Velocity Fields Comparison

The 3D velocity fields in both jets can only be assessed by means of advanced numerical models or experimental tests using complex measuring instrumentation, such as 3D laser-induced fluorescence. This section presents the main features of the flow patterns obtained by means of CFD simulations for the plunging and submerged jet. Both jets present a characteristic flow pattern for the same inflow momentum. The velocity vectors at $z = ½H$ of both jets can be observed in Figure 11, allowing a better understanding of the effect of the nozzle positions. Both positions generate a symmetric flow pattern in the y-axis.

The plunging jet breaks into droplets and falls, generating a void close to the wall, resulting in the jet separation, symmetrically, to the left and right. The divided jet continuously progresses, following the tank walls ('Coanda effect') until reuniting. After this, the jet proceeds as a reverse flow (in the outlet–inlet direction), crossing the centre of the tank until it reaches the inlet jet region (Figure 11a).

The main features of the submerged jet can be observed in Figure 11b. The submerged jet generates a long entrainment path, and as it reaches the wall, the jet is split symmetrically, in both directions (on the left and right sides), being clung to the tank walls. While it progresses, it reaches the inflow region and follows the same pattern.

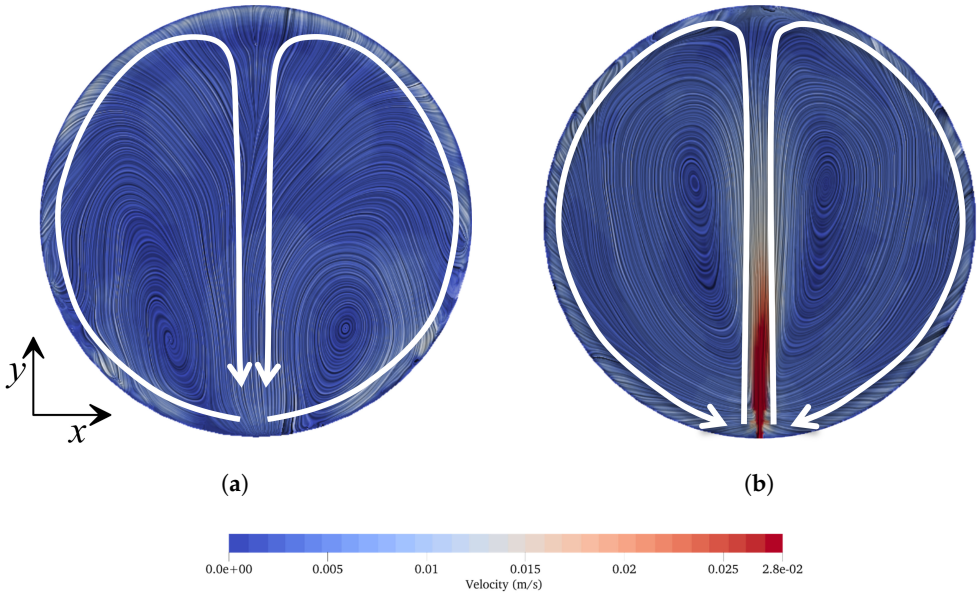

Figure 11. Flow pattern establishment and velocity fields at $z = 0.5H$ of the (**a**) plunging jet and (**b**) of the submerged jet.

The velocity magnitude at three distances from the inlet nozzle:$y = ¼\ D_T$; $½\ D_T$ and $¾\ D_T$, at three heights: $z = ¼$; ½ and ¾ H are plotted in Figure 12. Velocities in the submerged jet reach higher values than in the plunging jet. In addition, the entrainment path (jet spreading) can be identified by the considerable velocity magnitude spike at the $½\ H$, $y = ¼\ D_T$.

In the tank walls, the flow has a downward direction (Figure 10). In fact, this represents the primary air intake of the flow. For each disturbance in the tank, the water surface responds with a small pressure peak, causing waves in the surface that travels in the radial direction, going back and forward (walls–centre–walls). During these waves' impact on the tank walls, air bubbles are imprisoned and dragged by the downward flow into the storage water and observed into the outlet flow. In the pipe network, the air, in the form of bubbles, accumulates in high points as air pockets. This can be observed in both jets and is mainly responsible for the air pockets in the pipe network.

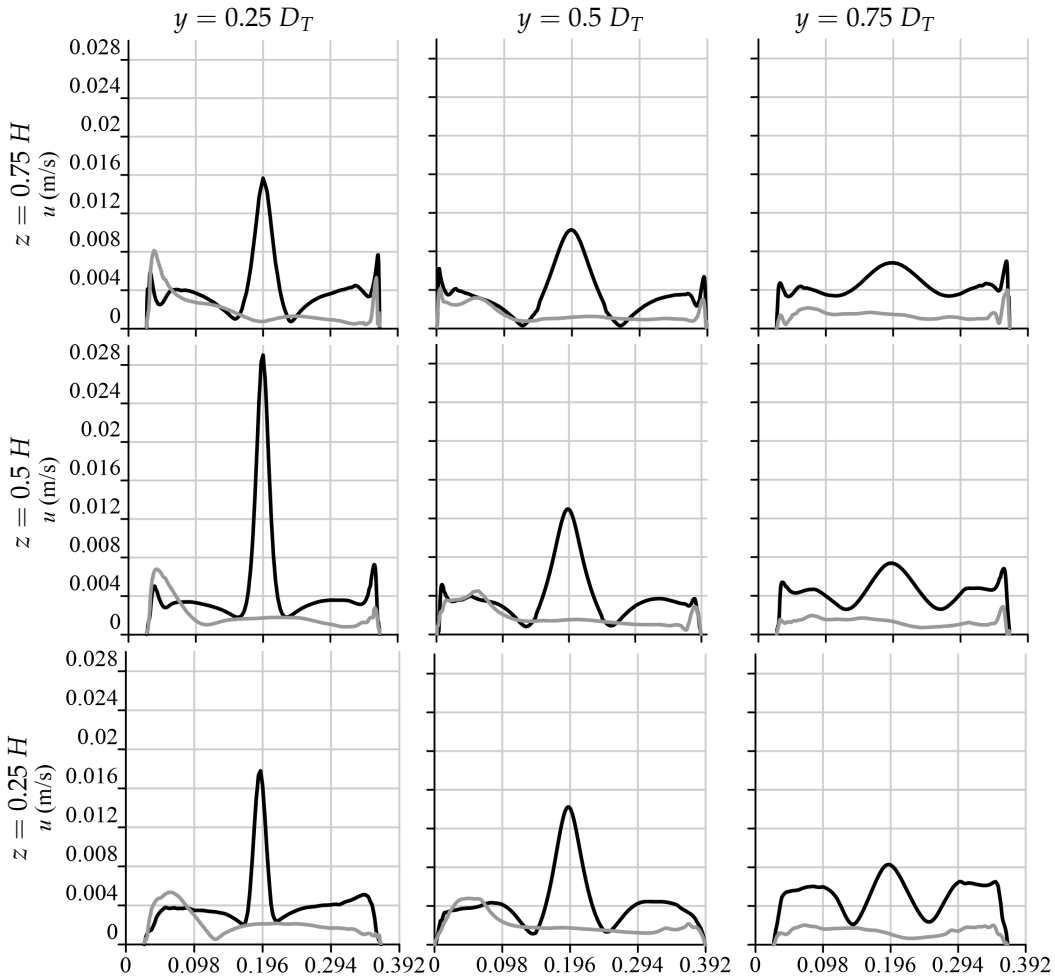

Figure 12. Velocity Profiles from: plunging jet—grey line; submerged jet—black line.

6. Conclusions

This research demonstrates that numerical models can capture the 3D behaviour of flow dynamics in water storage tanks. Two inlet jets' positions are analysed in a circular tank—the plunging jet (used to validate the CFD results qualitatively and configurations) and the submerged jet (a measure to improve water mixing)—for similar flow rate conditions.

CFD results allow assessing the influence of the nozzle position on the hydrodynamics conditions inside the tank. Each jet generates a preferential flow path or distinct flow pattern and velocity field in the water storage tank. The plunging jet breaks into droplets that fall into the water surface generating a void responsible for the progression of the jet clung to the tank wall and then produces a symmetrical flow clung to the walls and a flow in the centre of the tank. The submerged jet generates a long entrainment path with high velocities through the centre of the tank, promoting an enhanced water mixture by the turbulence created and a flow towards the inlet along the walls. In addition, pressure differences generate a small pressure peak in the water surface, creating an oscillatory motion (waves) that travels back and forward in the radial direction.

The molecular attraction forces of water molecules to each other (cohesion) and solids (adhesion) play an important role in the flow dynamics inside the storage tank. The plunging jet is highly influenced by the 'Coanda effect', being responsible for the early break of the jet into droplets and by its progression clung to the walls, as observed in the experimental tests carried out. The submerged jet tends to generate an entrainment path without the influence of the walls, spreading out as the nozzle distance increases.

Author Contributions: Conceptualization, N.M.C.M. and D.I.C.C.; methodology, N.M.C.M. and D.I.C.C.; validation, N.M.C.M. and D.I.C.C.; formal analysis, N.M.C.M. and D.I.C.C.; resources, N.M.C.M. and D.I.C.C.; data curation, N.M.C.M.; writing—original draft preparation, N.M.C.M. and D.I.C.C.; writing—review and editing, N.M.C.M. and D.I.C.C.; visualization, N.M.C.M. and D.I.C.C.; funding acquisition, N.M.C.M. and D.I.C.C. All authors have read and agreed to the published version of the manuscript.

Funding: This research was supported by Fundação para a Ciência e Tecnologia research projects: CPCA/A2/2568/2020—Flow Dynamics in Storage Tanks; PTDC/ECI-EGC/32102/2017—Improving Mixing in Storage Tanks for Safer Water Supply (IMiST); and DSAIPA/DS/0089/2018—Water Intelligence System Data.

Informed Consent Statement: Not applicable.

Data Availability Statement: Not applicable.

Data Availability Statement: All relevant data are included in the paper.

Acknowledgments: The authors would like to express a special acknowledgment to the Professor Emeritus António Betâmio de Almeida of Instituto Superior Técnico, Universidade de Lisboa, for fruitful discussions on the 'Coanda effect' and for the valuable suggestions that significantly improved the quality of this paper.

Conflicts of Interest: The authors declare no conflict of interest.

Abbreviations

The following abbreviations are used in this manuscript:

3D	Three-Dimensional
CFD	Computational Fluid Dynamics
SST	Shear Stress Transport

References

1. Panguluri, S.; Grayman, W.M.; Clark, R.M. *Water Distribution System Analysis: Field Studies, Modeling and Management: A Reference Guide for Utilities*; Report; U. S. Environmental Protection Agency: Washington, DC, USA, 2005.
2. Monteiro, L.S.P.P.; Viegas, R.M.C.; Covas, D.I.C.; Menaia, J.A.G.F. Assessment of Current Models Ability to Describe Chlorine Decay and Appraisal of Water Spectroscopic Data as Model Inputs. *J. Environ. Eng.* **2017**, *143*, 04016071. https://doi.org/10.1061/(ASCE)EE.1943-7870.
3. Mostafa, N.G.; Matta, M.E.; Halim, H.A. Simulation of Chlorine Decay in Water Distribution Networks Using EPANET—Case Study. *Civ. Environ. Res.* **2013**, *3*, 100–116.
4. Grayman, W.M.; Clark, R.M. Using Computer Models to Determine the Effect of Storage on Water Quality. *Am. Water Work. Assoc.* **1993**, *85*, 67–77. https://doi.org/10.1002/j.1551-8833.1993.tb06026.x.
5. Kennedy, M.S.; Moegling, S.; Sarikelle, S.; Surava, K. Assessing the Effects of Storage Tank Design on Water Quality. *Am. Water Work. Assoc.* **1993**, *85*, 78–88. https://doi.org/10.1002/j.1551-8833.1993.tb06027.x.
6. Fisher, I.; Sathasivan, A.; Chuo, P.; Kastl, G. Effects of stratification on chloramine decay in distribution system service reservoirs. *Water Res.* **2009**, *43*, 1403–13. https://doi.org/10.1016/j.watres.2008.12.012.
7. Bumrungthaichaichan, E.; Wattananusorn, S. CFD modeling of pump-around jet mixing tanks: A reliable model for overall mixing time prediction. *J. Chin. Inst. Eng.* **2019**, *42*, 428–437. https://doi.org/10.1080/02533839.2019.1598287.
8. Clark, R.M.; Abdesaken, F.; Boulos, P.F.; Mau, R.E. Mixing in Distribution System Storage Tanks: Its Effect on Water Quality. *J. Environ. Eng.-ASCE* **1996**, *122*, 814–821. https://doi.org/10.1061/(ASCE)0733-9372(1996)122:9(814).
9. Rossman, L.A.; Grayman, W.M. Scale-Model Studies of Mixing in Drinking Water Storage Tanks. *J. Environ. Eng.-ASCE* **1999**, *125*, 755–761. https://doi.org/10.1061/(asce)0733-9372(1999)125:8(755).
10. Olson, C.T.; DeBoer, D.E. *The Effects of Tank Operation and Design Characteristics on Water Quality in Distribution System Storage Tanks*; Report; Regional Water System Research Consortium: Brookings, SD, USA, 2011.
11. Duan, H.F.; Li, F.; Tao, T. Multi-objective Optimal Design of Detention Tanks in the Urban Stormwater Drainage System: Uncertainty and Sensitivity Analysis. *Water Resour. Manag.* **2016**, *30*, 2213–2226. https://doi.org/10.1007/s11269-016-1282-1.
12. Prasad, T.D.; Walters, G.A.; Savic, D.A. Booster Disinfection of Water Supply Networks: Multiobjective Approach. *J. Water Resour. Plan. Manag.* **2004**, *130*, 367–376. https://doi.org/10.1061/(ASCE)0733-9496(2004)130:5(367).
13. Angeloudis, A.; Stoesser, T.; Falconer, R.A. Predicting the disinfection efficiency range in chlorine contact tanks through a CFD-based approach. *Water Res.* **2014**, *60*, 118–129. https://doi.org/10.1016/j.watres.2014.04.037.

14. Musz-Pomorska, A.; Widomski, M.K. Modelling Studies of Water Chlorination Efficiency in Municipal Water Supply Network. *Ecol. Chem. Eng. A* **2020**, *27*, 1–13. https://doi.org/10.2428/ecea.2020.27(1-2)3.
15. Grayman, W.M.; Rossman, L.A.; Deininger, R.A.; Smith, C.D.; Arnold, C.N.; Smith, J.F. Mixing and Aging of Water in Distribution System Storage Failities. *AWWA* **2004**, *96*, 70–80. https://doi.org/10.1002/j.1551-8833.2004.tb10704.x.
16. Patwardhan, A.W. CFD modeling of jet mixed tanks. *Chem. Eng. Sci.* **2002**, *57*, 1307–1318. https://doi.org/Pii S0009-2509(02)00049-0.
17. Jaunâtre, J. Numerical Simulation of Threedimensional Flows in Water Storage Tanks—Application to Norra Ugglarps Reservoirs in South Sweden. Ph.D. Thesis, Lund University, Lund, Sweden, 2013.
18. Angeloudis, A.; Stoesser, T.; Kim, D.; Falconer, R.A. CFD Study of Flow and Transport Characteristics in Baffled Disinfection Tanks. In Proceedings of the 35th IAHR World Congress, Chengdu, China, 8–13 September 2013.
19. Stamatopoulos, K.; Alberini, F.; Batchelor, H.; Simmons, M.J.H. Use of PLIF to assess the mixing performance of small volume USP 2 apparatus in shear thinning media. *Chem. Eng. Sci.* **2016**, *145*, 1–9. https://doi.org/10.1016/j.ces.2016.01.032.
20. Tian, X.; Roberts, P.J. Mixing in Water Storage Tanks. I: No Buoyancy Effects. *J. Environ. Eng.-ASCE* **2008**, *134*, 974–985. https://doi.org/10.1061/(ASCE)0733-9372(2008)134:12(974).
21. Aparicio-Mauricio, G.; Rodriguez, F.A.; Pijpers, J.J.H.; Cruz-Diaz, M.R.; Rivero, E.P. CFD modeling of residence time distribution and experimental validation in a redox flow battery using free and porous flow. *J. Energy Storage* **2020**, *29*, 101337. https://doi.org/10.1016/j.est.2020.101337.
22. Martins, N.M.C.; Covas, D.I.C.; Meniconi, S.; Capponi, C.; Brunone, B. Characterisation of low-Reynolds number flow through an orifice: CFD results vs. laboratory data. *J. Hydroinform.* **2021**, *23*, 709–723. https://doi.org/10.2166/hydro.2021.101.
23. Martins, N.M.C.; Delgado, J.N.; Ramos, H.M.; Covas, D.I.C. Maximum transient pressures in a rapidly filling pipeline with entrapped air using a CFD model. *J. Hydraul. Res.* **2017**, *55*, 506–519. https://doi.org/10.1080/00221686.2016.1275046.
24. Martins, N.M.C.; Soares, A.K.; Ramos, H.M.; Covas, D.I.C. CFD modeling of transient flow in pressurized pipes. *Comput. Fluids* **2016**, *126*, 129–140. https://doi.org/10.1016/j.compfluid.2015.12.002.
25. Okita, N.; Oyama, Y. Mixing Characteristics in Jet Mixing. *Jpn. Chem. Eng.* **1963**, *27*, 252–260. https://doi.org/10.1252/kakoronbunshu 1953.27.252.
26. Khan, L.A.; Wicklein, E.A.; Teixeira, E.C. Validation of a Three-Dimensional Computational Fluid Dynamics Model of a Contact Tank. *J. Hydraul. Eng.-ASCE* **2006**, *132*, 741–746. https://doi.org/10.1061/(ASCE)0733-9429(2006)132:7(741).
27. Marek, M.; Stoesser, T.; Roberts, P.J.W.; Weitbrecht, V.; Jirka, G.H. CFD Modeling of Turbulent Jet Mixing in a Water Storage Tank. In Proceedings of the Congress-International Association for Hydraulic Research, Venice, Italy, 1–6 July 2007.
28. Zhang, J.P.; Huck, P.M.; Stubley, G.D.; Anderson, W.B. Application of a multiphase CFD modelling approach to improve ozone residual monitoring and tracer testing strategies for full-scale drinking water ozone disinfection processes. *J. Water Supply Res. Technol.* **2008**, *57*, 79–92. https://doi.org/10.2166/aqua.2008.038.
29. Xavier, M.L.M.; Janzen, J.G. Effects of inlet momentum and orientation on the hydraulic performance of water storage tanks. *Appl. Water Sci.* **2016**, *7*, 2545–2557. https://doi.org/10.1007/s13201-016-0449-5.
30. Tian, X.; Roberts, P.J. Mixing in Water Storage Tanks. II: With Buoyancy Effects. *J. Environ. Eng.-ASCE* **2008**, *134*, 986–995. https://doi.org/10.1061/(ASCE)0733-9372(2008)134:12(986).
31. Montoya Pachongo, C.; Laín Beatove, S.; Torres Lozada, P.; Cruz-Vélez, C.H.; Escobar Rivera, J.C. Effects of water inlet configuration in a service reservoir applying CFD modelling. *Ing. E Investig.* **2016**, *36*, 31–40. https://doi.org/10.15446/ing.investig.v36n1.50631.
32. Bonetto, F.; Lahey, R.T. An experimental study on air carryunder due to a plunging liquid jet. *Int. J. Multiph. Flow* **1993**, *19*, 281–294. https://doi.org/10.1016/0301-9322(93)90003-d.
33. Lezzi, A.M.; Prosperetti, A. The stability of an air film in a liquid flow. *J. Fluid Mech.* **1991**, *226*, 319–347.
34. Burgess, J.; Molloy, N.; McCarthy, M. A note on the plunging liquid jet reactor. *Chem. Eng. Sci.* **1972**, *27*, 442–445. https://doi.org/10.1016/0009-2509(72)85082-6.
35. Bonetto, F.; Lahey, R.T.; Drew, D.A. *An Experimental Study of Plunging Liquid Jet Induced Air Carryunder and Dispersion*; Center for Multyiphase, Rensselaer Polythecnic Institute: Troy, NY, USA 1993.
36. Labousse, M.; Bush, J.W.M. The hydraulic bump: The surface signature of a plunging jet. *Phys. Fluids* **2013**, *25*. https://doi.org/10.1063/1.4821360.
37. Sophocleous, M. Understanding and explaining surface tension and capillarity: An introduction to fundamental physics for water professionals. *Hydrogeol. J.* **2010**, *18*, 811–821. https://doi.org/10.1007/s10040-009-0565-5.
38. Lemanov, V.V.; Terekhov, V.I.; Sharov, K.A.; Shumeiko, A.A. An experimental study of submerged jets at low reynolds numbers. *Tech. Phys. Lett.* **2013**, *39*, 421–423. https://doi.org/10.1134/s1063785013050064.
39. Landa, P.S.; McClintock, P.V.E. Development of turbulence in subsonic submerged jets. *Phys. Rep.* **2004**, *397*, 1–62. https://doi.org/10.1016/j.physrep.2004.03.004.
40. Monteiro, L.; Pinheiro, A.; Carneiro, J.; Covas, D.I.C. Characterization of drinking water storage tanks in Portugal (in Portuguese). *Ing. Del Agua* **2021**, *25*, 49–58. https://doi.org/10.4995/ia.2021.13659.
41. Pinheiro, A.; Monteiro, L.; Carneiro, J.; do Céu Almeida, M.; Covas, D. Water Mixing and Renewal in Circular Cross-Section Storage Tanks as Influenced by Configuration and Operational Conditions. *J. Hydraul. Eng.* **2021**, *147*, 04021050. https://doi.org/10.1061/(asce)hy.1943-7900.0001955.

42. Wüthrich, B. Simulation and Validation of Compressible Flow in Nozzle Geometries and Validation of OpenFOAM for This Application. Master's Thesis, Swiss Federal Institute of Technology Zurich, Zürich, Switzerland, 2007. https://doi.org/10.3929/ethz-a-005575219.
43. Holzmann, T. *Mathematics Numerics Derivations And OpenFOAM (v7) The Basics for Numerical Simulations*; Holzmann CFD: Loeben, Germany, 2019. https://doi.org/10.13140/RG.2.2.27193.36960.
44. Zalesak, S.T. Fully Multidimensional Flux-Corrected Transport Algorithms for Fluids. *J. Comput. Phys.* **1979**, *31*, 335–362. https://doi.org/10.1016/0021-9991(79)90051-2.
45. Denton, J.D.; Dawes, W.N. Computational fluid dynamics for turbomachinery design. *Proc. Inst. Mech. Eng. Part C J. Mech. Eng. Sci.* **1998**, *213*, 107–124. https://doi.org/10.1243/0954406991522211.
46. Menter, F.R.; Kuntz, M.; Langtry, R. Ten years of industrial experience with the SST turbulence model. *Turbul. Heat Mass Transf.* **2003**, *4*, 625–632.
47. El Halal, Y.; Marques, C.; Rocha, L.; Isoldi, L.; Lemos, R.; Fragassa, C.; dos Santos, E. Numerical Study of Turbulent Air and Water Flows in a Nozzle Based on the Coanda Effect. *J. Mar. Sci. Eng.* **2019**, *7*, 21. https://doi.org/10.3390/jmse7020021.
48. Giles, B.D. Fluidics, the Coanda Effect, and some orographic winds. *Arch. Meteorol. Geophys. Bioklimatol. Ser. A* **1977**, *25*, 273–279. https://doi.org/10.1007/bf02321800.
49. Hegde, M. *Fluid Mechanics and the Plateau-Rayleigh Instability*; Report; University of California: Burkley, CA, USA, 2013
50. Tran, T.; de Maleprade, H.; Sun, C.; Lohse, D. Air entrainment during impact of droplets on liquid surfaces. *J. Fluid Mech.* **2013**, *726*. https://doi.org/10.1017/jfm.2013.261.
51. Cervantes-Alvarez, A.M.; Escobar-Ortega, Y.Y.; Sauret, A.; Pacheco-Vazquez, F. Air entrainment and granular bubbles generated by a jet of grains entering water. *J. Colloid Interface Sci.* **2020**, *574*, 285–292. https://doi.org/10.1016/j.jcis.2020.04.009.
52. Qu, X.L.; Khezzar, L.; Danciu, D.; Labois, M.; Lakehal, D. Characterization of plunging liquid jets: A combined experimental and numerical investigation. *Int. J. Multiph. Flow* **2011**, *37*, 722–731. https://doi.org/10.1016/j.ijmultiphaseflow.2011.02.006.
53. Martin, C.I.; Matioc, B.V. Existence of Wilton Ripples for Water Waves with Constant Vorticity and Capillary Effects. *SIAM J. Appl. Math.* **2013**, *73*, 1582–1595. https://doi.org/10.1137/120900290.